# Interpolation between plant responses in a head-tracked local active noise control headrest system.

Francesco Veronesi, Chung Kwan Lai, Jordan Cheer\*

<sup>a</sup>Institute of Sound and Vibration Research, University of Southampton, University Road, Southampton, SO17 1BJ, Hampshire, United Kingdom

#### **Abstract**

Active Noise Control (ANC) headrest systems reduce noise at the listener's ears, but their performance can degrade with user movement. Integrating head-tracking into Local ANC systems improves performance over a wider frequency range by updating the controller for different head positions and orientations. However, practical implementations often rely on a limited set of pre-calibrated system response models, resulting in mismatches between actual and modelled head positions. Increasing the resolution of the measurement grid can mitigate this, but increases the complexity of pre-calibration. This study investigates interpolation strategies - such as inverse distance weighting, high-degree and cubic spline interpolation - to estimate plant responses between pre-calibrated positions and improve control performance. The effects of interpolation are analysed by evaluating the condition number and noise reduction achieved, with separate interpolation applied for head translations and rotations. The findings show that accurate methods, such as cubic spline and high-degree interpolation, produce more accurate plant models, which improve controller robustness, particularly at higher frequencies. In addition, frequency-dependent regularisation maximises control performance, with accurate interpolation requiring less regularisation to achieve greater noise reduction. These findings highlight the importance of selecting appropriate interpolation methods and strategic pre-calibration grid designs to ensure effective ANC system performance.

Keywords: Interpolation, Active Headrest, Active Noise Control, Head-tracking

## 1. Introduction

Low-frequency sounds are becoming increasingly recognised as a health hazard and a cause of discomfort, fatigue and loss of concentration [1]. However, since passive mitigation methods generally become massive and bulky when they are used to control low frequency sounds, active control strategies for reducing noise have been investigated over an extended period of time [2]. Active Noise Control (ANC) has been applied in a variety of fields, including in the automotive environment, in aircraft and in headphones [1]. This paper focuses on active headrest systems, which are designed to reduce noise at the ears of a seated listener using a set of loudspeakers attached to the headrest. These systems do not generally achieve as high a level of control performance as headphone based systems, but provide the user with a potentially greater level of comfort and freedom.

In recent years, a number of different controller designs have been proposed for headrest systems [3, 4, 5, 6]. A limited number of these studies, however, investigate the effect of head movements on the overall performance of the local control system [3, 7, 8, 9, 10, 11], a topic that is of particular practical relevance when the user is free to move within the headrest. Indeed, despite offering a potential increase in the control bandwidth compared to global control strategies, local control is limited to a region of space around each error microphone. It has been shown that this so-called zone of quiet is around 1/10-th of the acoustic wavelength wide in a diffuse sound field [12, 13]. Thus, while significant attenuation may be achieved at the physical sensor locations, a listener may have the impression of moving in and out of a region of silence, which may be more annoying than the original uncontrolled disturbance [7, 14].

<sup>\*</sup>j.cheer@soton.ac.uk

In a conventional active headrest without head-tracking, the noise attenuation at the user's ears will decrease significantly as the head moves away from the error sensor locations [15]. To counteract this effect, and attain control stability that is robust to variations in the controlled system [16], different strategies have been proposed [10, 14, 15, 17, 18, 19]. In the context of active headrests, it has variously been shown that it is possible to overcome this limitation by moving the quiet zones by updating the controller based on information provided by an optical device able to track head movements [3, 7, 10, 20, 21, 22]. In this scenario, the head-tracker is used to identify the position and orientation of the head and accordingly update the controller to maintain control at the user's ears. For a typical feedforward controller, the modelled plant responses and either the disturbance signals, or the observation filters used to estimate the disturbance signals are updated [4]. For the case where it is assumed that the disturbance field is static, then both the disturbance and the modelled plant responses are pre-determined during an identification stage, ideally for all head positions and orientations [10, 23]. In practice, however, the number of head positions and orientations for which the plant responses are measured in advance must be finite and, therefore, during control there will be some error between the physical head position and the nearest head position for which the plant responses were measured during the identification phase. The spatial sampling of the plant responses for different head positions might typically be carried out on a grid with a spacing between measurement positions of a few centimetres. Indeed, at wavelengths larger than the dimension of the head, the zone of quiet coincides with that obtained in a free diffuse sound field [24, 25], and thus for a -10 dB noise reduction up to 700 Hz a spatial sampling resolution of 2.5 cm is expected to be sufficient [7]. However, at higher frequencies the "extent" and shape of the zone of quiet changes due to the scattering of sound by a reflecting surface [25], and thus, for the mitigation of higher frequency sounds the required measurement grid resolution will increase and lead to an extremely lengthy identification procedure. This results in the need to store significant numbers of plant responses in memory. To reduce this requirement, this paper presents an investigation into the use of interpolation strategies to estimate the plant models at head positions in between the positions measured during the identification stage.

In the field of binaural synthesis, research into interpolation between Head-Related Transfer Functions (HRTFs) has been variously investigated. Interpolation algorithms for spherical data representing HRTFs have been discussed by many authors [26, 27, 28, 29] and may be distinguished with respect to whether they operate on neighbouring data points only (nearest neighbour, polynomials), or whether they require a full-spherical data set (inverse distance weighting, splines) [30]. More broadly, interpolation has also been investigated for 3D data across a variety of fields, including geophysics and digital image processing [31, 32, 33]. However, in the context of ANC, interpolation between plant responses associated with moving error microphones has only seen relatively modest levels of investigation in the literature. In particular, in this work [18] interpolation is investigated for the control of a narrowband noise in a one-dimensional duct, and in this study [14] interpolation is investigated for noise control at the ears of a rotating head in a three-dimensional cavity. In this latter work, the virtual error signal at the moving virtual location is estimated by interpolating the virtual error signals, but no details are provided regarding the interpolation algorithm that is used. Interpolation has also been applied to improve the accuracy of sound field estimation between error microphones in the context of spatial ANC [34, 35]. In active headrests, however, interpolation methods for enhancing noise reduction at the listener's ears have received relatively little attention. While some work has been done on the use of interpolation in head-tracking-equipped active headrests, these studies simply demonstrate the feasibility of implementing interpolation methods rather than investigating how different interpolation algorithms affect control performance [36, 11]". Other studies on active headrests have emphasised the importance of interpolation in improving noise reduction when the listener's head is not in a measured position [21, 22], or when control is performed with virtual sensing algorithms, where the target areas are located remotely from the microphone positions [37, 38, 39]. Combining interpolation with such algorithms can have a significant impact, as demonstrated in related applications [18, 34], thereby underlining the relevance of the following analysis.

To provide further insight into the use of interpolation between the plant responses associated with a headrest ANC system with a moving head, this paper presents a systematic review and comparison of different interpolation algorithms that could be used to increase the accuracy of the plant models. To this end, the work is organised as follows. In Section 2 the ANC headrest system and the assumed feedforward control algorithm are described; Section 3 describes the interpolation problem and presents the considered two-dimensional interpolation strategies. Section 4 presents a comparison between the plant responses estimated using the different interpolation strategies, while Section 5 investigates the effect that the interpolation strategies have on control performance. Finally, Section 6 summarises

the paper and draws conclusions.

## 2. Active headrest and control algorithm

Active headrest systems are designed to attenuate noise around a person's ears [5]. This is typically achieved through the use of a set of loudspeakers positioned in close proximity to the head, which are driven with control signals that are determined by a controller designed to minimise the pressures monitored by a set of microphones. This section describes the active headrest system under consideration and the control algorithm employed.

## 2.1. Active headrest system description and plant identification

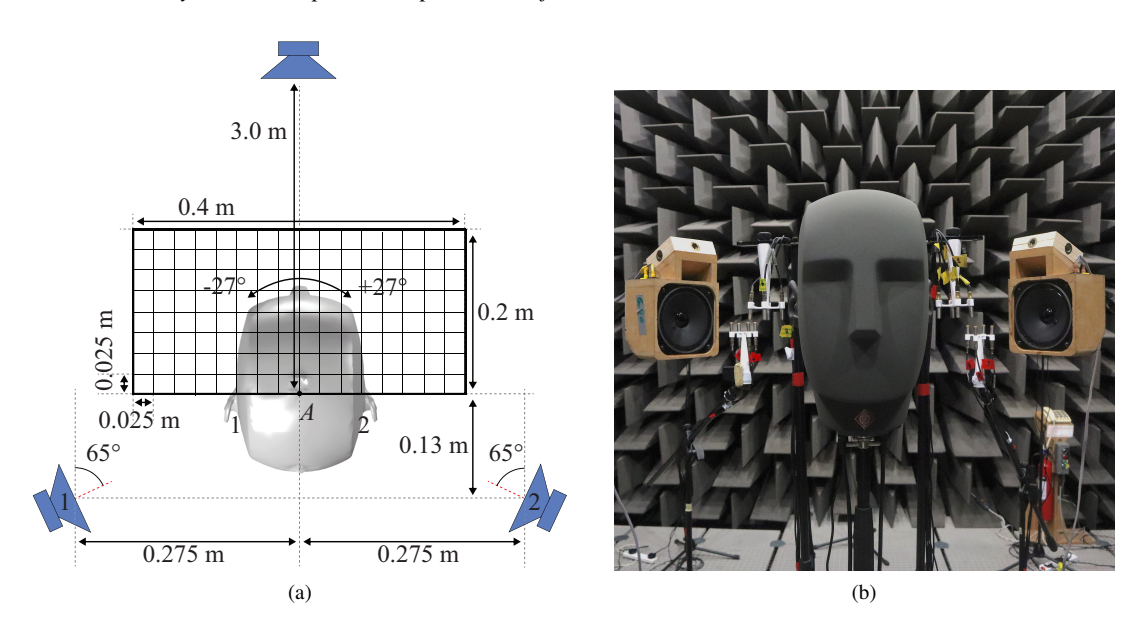


Figure 1: Illustration showing the layout of the control system (a) and a picture of the experimental realisation (b). Please note, the microphones that are visible in figure (b) close to the dummy head were not utilised in this work. The error signals are measured with the in-ear Neumann KU 100 microphones.

The headrest system considered consists of a primary acoustic source, two secondary loudspeakers, and two error microphones, which are assumed to be mounted inside the ears of the dummy head (Neumann KU 100). Figure 1 illustrates the spatial arrangement of these system components, both diagrammatically and with a photograph of the experimental implementation. The primary source utilised in this study is situated at a distance of three metres from the nominal head position, which will be denoted A in the text. A Genelec 8030a loudspeaker, with the tweeters aimed at the dummy head is used as the primary source. The secondary sources are located 55 cm apart at a distance of 13 cm behind the nominal head position. The loudspeakers employed are passive and are mounted in small wooden cabinets, inclined by 65° so that they are pointing towards the ears of the dummy head when it is located at the nominal position. The secondary loudspeakers utilise Visaton-R 10 S drivers.

The plant responses between the active headrest secondary sources and error microphones have been measured between 150 and 1500 Hz, using the swept-sine method, with the head located at discrete spatial positions and rotations. Head translations are constrained within a 40 cm  $\times$  20 cm grid, divided into 153 fixed measurement locations spaced 2.5 cm apart (cf. Figure 1a). Since ground truth plant responses are necessary to evaluate the accuracy of interpolation, plant responses are interpolated between head translations at grid points spaced at integer multiples of 5 cm or 10 cm from the nominal position A, and the plant responses corresponding to the midpoints of the 5 cm or 10 cm grid are used as the ground truth. The yaw angular displacement of the head is constrained to a maximum of  $\pm$ 27° and is sampled at intervals of 9°. The maximum rotational angle under consideration is slightly lower than that chosen in [14]. Interpolation between head rotations is performed by interpolating plant responses at 0° and  $\pm$ 27°,

and thus the responses measured for head rotations of  $\pm 9^{\circ}$  and  $\pm 18^{\circ}$  represent the ground truth. In this paper, heave (up-down) translational movements, together with pitch and roll rotations, are not considered in order to constrain the problem and focus on head movements more likely to occur in an active headrest system. With this assumption, head configurations within the tracking grid can be described by means of the vector  $\psi = (x, y, \theta)$ , where the Cartesian coordinates x and y define surge (front-back) and sway (left-right) head movements from the nominal position A respectively, and  $\theta$  indicates head rotation measured in a clockwise direction. As described above, the head position and rotation are discretised and so the variables  $\psi_{n,m,l}$  and  $(\mathbf{r}_{n,m}, \theta_l)$  will be used to define the discrete spatial and angular head configuration  $(x_n, y_m, \theta_l)$ .

## 2.2. Multichannel local control of a tonal disturbance

In this work, it is assumed that the primary noise is a pure tone disturbance and that the plant is linear. These assumptions allow for the implementation of a frequency domain tonal controller, which assumes that there is no constraint on causality and that a perfect reference signal is available. This provides useful physical insight into the limitations of control, without making specific assumptions about the reference signal acquisition and properties. The primary source generates two complex disturbance signals at the two error sensors, which are represented, at a given frequency, by the vector  $\mathbf{d}$ , while the two secondary sources are driven by the vector of control signals  $\mathbf{u}$ . If the  $2 \times 2$  matrix of complex frequency responses between the left and right loudspeakers and the left and right ears at a given frequency is denoted  $\mathbf{G}$ , then the vector of residual error signals in the steady state can be expressed as [13]

$$e = d + Gu. (1)$$

In fixed ANC systems, i.e., where the plant is time invariant, the optimal input to the secondary sources,  $u_{opt}$ , can be found in a least mean-squares sense by considering the error signal defined in Equation (1). However, in the active headrest system under investigation, where the head is free to move and rotate, the matrix of physical plant responses, G, is not always available. Consequently, the control algorithm must utilise an estimate of G, namely  $\hat{G}$ , known as the plant model. In this case, the optimal control signal is found by minimising the cost function [13]

$$J = \hat{\boldsymbol{e}}^H \hat{\boldsymbol{e}} + \beta \boldsymbol{u}^H \boldsymbol{u},\tag{2}$$

where  $\hat{e} = d + \hat{G}u$  defines the estimated error signals, and H denotes the Hermitian transpose. In Equation (2), the regularisation parameter  $\beta$ , known as the effort-weighting parameter, determines the relative weight assigned to the control effort  $u^H u$ , which is proportional to the electrical power required to drive the secondary sources [13]. As  $\beta$  changes from zero to infinity, the solution changes from minimising only the performance error to minimising the control effort [40]. Appropriate tuning of the effort-weighting parameter enables a trade-off between the accuracy with which the disturbance signals are cancelled at the error sensors and the robustness of this cancellation to errors in the plant model [23]. The minimisation of the cost function defined in (2) yields the optimal control signals

$$\boldsymbol{u}_{\text{opt}} = -[\hat{\boldsymbol{G}}^H \hat{\boldsymbol{G}} + \beta \boldsymbol{I}]^{-1} \hat{\boldsymbol{G}}^H \boldsymbol{d}. \tag{3}$$

Previous studies have shown that using control signals calculated according to Equation (3) in a head-tracked active headrest system allows useful levels of noise attenuation to be achieved up to around 1 kHz, but this work assumes that during control the dummy head is located at positions corresponding to the grid over which the plant response models have been measured during a calibration phase [7] and, therefore,  $\hat{G} = G$ . In reality, however, the head would be free to move continuously between the discretised grid positions and, therefore, when the head is not collocated with a grid position,  $\hat{G}$  will be inaccurate and there will be an error between the physical and modelled plant responses. To help overcome this limitation without requiring a finer measurement grid to be utilised during the plant model calibration phase, interpolation can be employed to improve the accuracy of the plant models. The optimal control signals in this case will be defined here as

$$\mathbf{u}_{\underset{\sim \text{opt}}{\sim}} = -[\hat{\mathbf{G}}^H \hat{\mathbf{G}} + \beta \mathbf{I}]^{-1} \hat{\mathbf{G}}^H \mathbf{d}, \tag{4}$$

where  $\hat{G}$  is the plant model estimated by interpolating between measured plant models,  $\hat{G}$ . In a practical implementation, the head-tracker would determine the head position and orientation in real-time, typically utilising some form

of optical tracking method [41], and use it to update the current head configuration,  $\psi$ , within the tracking grid. The principle of operation would then be identical to that presented in [3, 4, 7], with the addition of an interpolation block in the control algorithm. The use of interpolation is expected to increase the accuracy of the estimation of G, thereby also enhancing control performance. Equation (4) will be employed to investigate the effect of plant response interpolation on the control performance and to determine how in the presence of interpolation the regularisation parameter  $\beta$  influences the robust performance of the controller.

#### 3. Interpolation strategies

In the context of active headrest systems, previous research has revealed significant changes in the plant responses for different head positions and rotations. For example, it has been shown that, for the same headrest under investigation here, such differences are distinct between the ipsilateral and contralateral path [3]. Overall, it emerges that the magnitude and phase responses of the direct path vary significantly between different head configurations, while preserving a consistent spectral shape, largely due to changes in the distance between the loudspeaker and the ear. Similar variations are observed in the cross-path in relation to head position and rotation. However, in the frequency range above 1 kHz, plant response variations are highly influenced by head shadowing effects. Analogous analyses were previously reported [4], which demonstrated the importance of tracking head movements and updating the plant response model in order to avoid excessive regularisation. These studies emphasise the necessity to consider interpolation to achieve more accurate plant models, and potentially enhance control performance.

This section introduces the considered interpolation strategies that will be used to evaluate the effect of interpolation on the accuracy of the plant models and assess the influence that this has on control performance. These strategies include Nearest Neighbour (NN) interpolation, Inverse Distance Weighting (IDW) or Shepard interpolation, High-Degree (HD) or polynomial interpolation, and Cubic Spline interpolation. These interpolation strategies have been selected to provide a range of levels of potential complexity and are also commonly tested and compared in the somewhat related context of binaural audio, where spherical data such as HRTFs are used [27, 29]. This section will focus exclusively on the two-dimensional formulations and examine the approach used to interpolate between different head translations, since the application to head rotations is straightforward.

# 3.1. Nearest Neighbour interpolation

Nearest Neighbour (NN) interpolation is the approach taken in previous head-tracked local ANC systems to estimate the plant response matrix at head positions that do not coincide with the grid positions for which the plant matrix was measured during the calibration [4, 7]. Specifically, the frequency response of the plant at the coordinate position  $\tilde{r}$  is approximated using the frequency response of the plant measured at the nearest neighbour coordinate location  $r_{n,m}$ , i.e.,

$$\hat{G}(\widetilde{r}) = \hat{G}(r_{n,m}), \text{ for } r_{n,m}: \min_{n,m} ||\widetilde{r} - r_{n,m}||_2$$

$$(5)$$

where  $\|\cdot\|_2$  denotes the Euclidean norm. Due to its definition, NN interpolation is considered by some texts as a non-interpolation approach [30]. However, it remains useful in applications where computational limitations exist.

In cases where the head position,  $\tilde{r}$ , lies exactly at the midpoint of four adjacent grid points, or between two adjacent points, it is necessary to introduce a selection criterion for determining the nearest neighbour. In this paper, the nearest neighbour selected is the one that most accurately represents the actual plant response at the head location, measured in terms of the Euclidean norm of the difference between the responses measured at  $\tilde{r}$  and at each of the equidistant grid points. Although this is not practical, since the response at  $\tilde{r}$  would not be known, it provides a best case scenario for this approach.

# 3.2. Inverse Distance Weighting interpolation

Inverse Distance Weighting (IDW) interpolation, devised by Shepard[42], estimates the plant response G at the point  $\tilde{r}$  using a weighted sum of all the measured plant responses, with the weighting depending on the distance between the estimation position and the measurement positions. According to the interpolation algorithm, the weights

are specifically given by a power of the inverse of the Euclidean distance between the estimation point  $\tilde{r}$  and the measurement points  $r_{n,m}$ . Thus, IDW interpolation of power  $\gamma \geq 0$  states that

$$\hat{G}(\widetilde{\boldsymbol{r}}) = \begin{cases} \frac{\sum\limits_{n,m} w_{n,m}^{-\gamma} \cdot \hat{G}(\boldsymbol{r}_{n,m})}{\sum\limits_{n,m} w_{n,m}^{-\gamma}}, & \text{if } w_{n,m} \neq 0 \ \forall n,m\\ \hat{G}(\boldsymbol{r}_{n,m}), & \text{if } \exists n,m: \ w_{n,m} = 0. \end{cases}$$

$$(6)$$

Equation (6) shows that the weight  $w_{n,m} = ||\tilde{r} - r_{n,m}||_2^{-\gamma}$  decreases as the distance between  $\tilde{r}$  and  $r_{n,m}$  increases. Thus, greater values of  $\gamma$  assign greater influence to values closest to the interpolated point. In particular, it can be shown that IDW turns into NN interpolation for  $\gamma \gg 2$ . On the other hand, power parameters  $\gamma \le 2$  cause the interpolated values to be dominated by points far away. Therefore, values of  $\gamma$  between 2 and 6 are recommended [43, 44]. IDW is particularly well suited for the graphical representation of surfaces, especially when grid nodes are arranged in a completely arbitrary and unordered manner. However, IDW is a global interpolation method, as all available data points are used to calculate each new functional value  $\hat{G}(\tilde{r})$ , and thus it demands a high level of computation. Modifications to this interpolation strategy, which only use nodes within a circle of a given radius, have been proposed [43], but will not be investigated in this work since the differences in behaviour and performance are not significantly distinct from straightforward IDW.

## 3.3. High-Degree interpolation

For one dimensional data, High-Degree (HD) or polynomial interpolation uses the lowest possible degree polynomial to fit a function at a given point by passing through the available neighbouring points that belong to the data set. Therefore, in order for this polynomial to be correctly estimated, the algorithm uses a number of measured points equal to  $\delta + 1$ , where  $\delta$  is the degree of the polynomial. In the two-dimensional case, HD interpolation is implemented by intermediating the result of two one-dimensional interpolations using a number of measured points equal to  $(\delta_x + 1)(\delta_y + 1)$ , where  $\delta_x$  and  $\delta_y$  are the degrees of the polynomials along the x and y directions respectively.

In order to calculate the plant estimate,  $\hat{G}$ , at point  $\tilde{r}$ , HD interpolation uses a group of selected adjacent points, namely  $(x_{n+q_x}, y_{m+q_y})$ , where the values of  $q_x$  and  $q_y$ , which are integer values, vary in accordance with the interpolation degree. Figure 2 illustrates how these points are selected according to the degree of interpolation. HD interpolation calculates the value of  $\hat{G}$  at point  $\tilde{r}$  using the following process [45],

$$\hat{G}(\widetilde{x}, y_m) = \sum_{q_x} \hat{G}(x_{n+q_x}, y_m) L_{q_x}(s_{\widetilde{x}})$$
(7a)

$$\hat{G}(\widetilde{x}, \widetilde{y}) = \sum_{q_{x}} \hat{G}(\widetilde{x}, y_{m+q_{y}}) L_{q_{y}}(s_{\widetilde{y}}), \tag{7b}$$

where  $(x_n, y_m)$  is the grid point closest to  $(\widetilde{x}, \widetilde{y})$  that satisfies the conditions  $x_n \leq \widetilde{x} < x_{n+1}$ , and  $y_m \leq \widetilde{y} < y_{m+1}$  (see Figure 2 for reference); the function  $G(\widetilde{x}, y_m)$  represents the intermediate interpolation result along the  $m + q_y$  grid line,  $L_{q_x}(s)$  and  $L_{q_y}(s)$  respectively denote the 'row' and 'column' convolution coefficients (also known as kernel or Lagrange basis functions), and the coefficients  $s_{\widetilde{x}}$  and  $s_{\widetilde{y}}$  are the normalised distances between  $\widetilde{r}$  and  $r_{n,m}$  [46], which can be expressed as

$$\begin{cases} s_{\widetilde{x}} = \frac{\widetilde{x} - x_n}{x_{n+1} - x_n} \\ s_{\widetilde{y}} = \frac{\widetilde{y} - y_m}{y_{m+1} - y_m}. \end{cases}$$
(8)

Equation (7) shows that two-dimensional HD interpolation is performed in two steps. In the first step, interpolation is performed  $\delta_y + 1$  times exclusively along the x-axis, i.e., by considering values of  $\hat{G}$  at grid points  $(x_{n+q_x}, y_{m+q_y})$ , where  $q_y$  is fixed. In the second step, the functions  $\hat{G}(\widetilde{x}, y_{m+q_y})$  obtained from stage one are used for a final interpolation

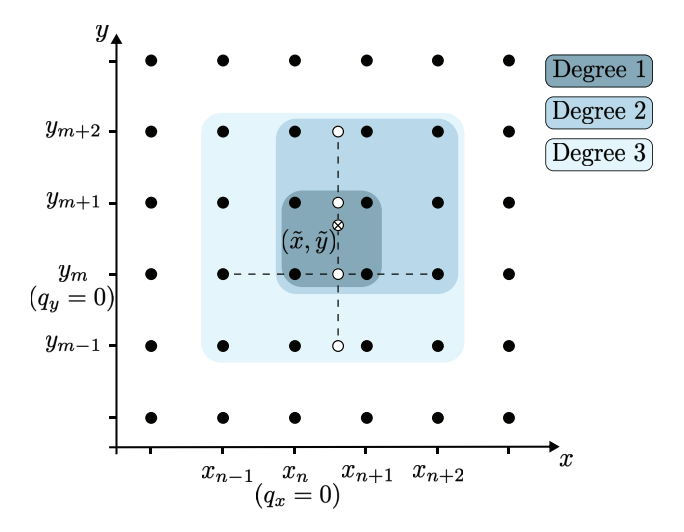


Figure 2: Illustration of sampling points in high-degree interpolation: black dots are sample function values, white circles represent intermediate results, and the white dot with a cross marks the interpolation point.

along the y-axis. In other words, the interpolation algorithm illustrated in Equation (7) consists of several independent row-direction one-dimensional interpolations (7a) and one column-direction interpolation (7b) [45]. The algorithm is quite general and works regardless of the number of points that are chosen along the two directions. One may in fact decide to perform degree-1 interpolation along the x direction and degree-3 interpolation along the y direction. Thus, the resulting  $\hat{G}(x, y)$  will vary according to the selected strategy. It is therefore up to the user to decide which interpolation degree best fits the properties of the function that is to be interpolated.

The kernel functions,  $L_{q_x}(s_{\widetilde{x}})$  and  $L_{q_y}(s_{\widetilde{y}})$ , used in the HD interpolation defined by Equation (7) are distinct for the three different interpolation degrees and are defined as follows. For conciseness, only the kernel functions in the x direction will be presented here, as those used in the y-direction are equivalent.

## (i) Linear interpolation (Degree-1 Interpolation)

The kernel function of degree-1 interpolation is defined as [45, 47],

$$L_{q_x}(s_{\overline{x}}) = \begin{cases} 1 - s_{\overline{x}}, & \text{if } q_x = 0\\ s_{\overline{x}}, & \text{if } q_x = 1 \end{cases}$$

$$\tag{9}$$

Figure 2 shows that two-dimensional linear interpolation, or bilinear interpolation, involves two row directions and one column direction convolution as per Equation (7), which results in a computation that requires knowledge of  $\hat{G}$  at four grid points [45]. Equation (8) states that the coefficients  $s_{\tilde{x}}$  and  $s_{\tilde{y}}$  are normalised, i.e. they lie between 0 and 1 [46]. In particular,  $s_{\tilde{x}}$  and  $s_{\tilde{y}}$  are either 0 or 1 exclusively in cases where the point  $\tilde{r}$  is equal to one of the grid points. From this it follows that bilinear interpolation is a kind of weighted average between four different values. Hence, the interpolation error is greatest when  $\tilde{r}$  lies exactly in the middle of the cell, and that it becomes larger when the gradient between the four involved points is greater.

Finally, it should be emphasised that bilinear interpolation performed on a rectangular grid is equivalent to Natural Neighbour (or Sibson) interpolation with Voronoi weights, firstly introduced in [48] and used by several authors for the interpolation of HRTFs [26].

#### (ii) Ouadratic interpolation (Degree-2 Interpolation)

The quadratic polynomial kernel that is used for degree-2 interpolation is given by [45]

$$L_{q_{x}}(s_{\widetilde{x}}) = \begin{cases} \frac{1}{2}s_{\widetilde{x}}^{2} - \frac{3}{2}s_{\widetilde{x}} + 1, & \text{if } q_{x} = 0\\ -s_{\widetilde{x}}^{2} + 2s_{\widetilde{x}}, & \text{if } q_{x} = 1\\ \frac{1}{2}s_{\widetilde{x}}^{2} - \frac{1}{2}s_{\widetilde{x}}, & \text{if } q_{x} = 2 \end{cases}$$
 (10)

where  $x_n \le \widetilde{x} \le x_{n+2}$  and  $x_n < x_{n+1} < x_{n+2}$ . Differently from the previous case, two-dimensional quadratic interpolation, or biquadratic interpolation, requires three row directions and one column direction convolution, and thus the need to know  $\hat{G}$  at nine grid points (cf. Figure 2). Consequently, biquadratic interpolation cannot always be applied and extrapolation methods must be implemented to estimate  $\hat{G}$  outside the grid boundaries.

## (iii) Cubic interpolation (Degree-3 Interpolation)

Lastly, the cubic Lagrange kernel that is used for the degree-3 interpolation is defined as [45]

$$L_{q_{x}}(s_{\widetilde{x}}) = \begin{cases} -\frac{1}{6}s_{\widetilde{x}}^{3} + \frac{1}{2}s_{\widetilde{x}}^{2} - \frac{1}{3}s_{\widetilde{x}}, & \text{if } q_{x} = -1\\ \frac{1}{2}s_{\widetilde{x}}^{3} - s_{\widetilde{x}}^{2} - \frac{1}{2}s_{\widetilde{x}} + 1, & \text{if } q_{x} = 0\\ -\frac{1}{2}s_{\widetilde{x}}^{3} + \frac{1}{2}s_{\widetilde{x}}^{2} + s_{\widetilde{x}}, & \text{if } q_{x} = 1\\ \frac{1}{6}s_{\widetilde{x}}^{3} - \frac{1}{6}s_{\widetilde{x}}, & \text{if } q_{x} = 2 \end{cases}$$

$$(11)$$

where  $x_{n-1} \le \widetilde{x} \le x_{n+2}$  and  $x_{n-1} < x_n < x_{n+1} < x_{n+2}$ . As illustrated in Figure 2, two-dimensional cubic interpolation, or bicubic interpolation, requires four row directions and one column direction convolution, and thus the need to know  $\hat{G}$  at 16 nodes. For this reason, similarly to biquadratic interpolation,  $\hat{G}$  has to be extrapolated outside the grid boundaries.

High-Degree interpolation methods are excellent if the interpolation degree is equal to the degree of the polynomial that has to be interpolated. However, they are inefficient when the function is characterised by singularities, ripples or behaviour that would require a polynomial of infinite degree to be approximated. For this reason, to limit the number of variables and minimise interpolation error, it is assumed throughout the paper that  $\delta_x = \delta_y$ . Furthermore, HD interpolation is ineffective at points along the grid boundary where extrapolation strategies are employed. This has a detrimental effect on the estimation of plant responses, thus requiring the user to investigate and implement more accurate extrapolation methods. Hence, to approximate functions of several variables the use of multidimensional splines is recommended [43]. It is also worth noting that although this class of interpolation strategy guarantees the continuity of the interpolated function, it does not ensure continuity of the gradient [46]. In particular, the value of the function  $\hat{G}(\vec{r})$  changes continuously as the position of the point  $\vec{r}$  varies. However, its gradient changes discontinuously at the boundaries of the region of  $(\delta_x + 1)(\delta_y + 1)$  points considered for interpolation. Consequently, as the interpolation degree increases, the contour of the region along which the gradient of the estimated function is discontinuous also increases. Thus, HD interpolation does not solve the discontinuity problem of the gradient that is observed for NN and IDW interpolation, but increases the distance between the points where such discontinuity occurs.

# 3.4. Bicubic spline interpolation

The final interpolation strategy that will be considered here is bicubic spline interpolation. Similar to IDW interpolation, bicubic spline is a global method, requiring both the use and knowledge of the interpolated values across the entire domain. A general concise description of this interpolation strategy is presented, and the is reader referred to key references [49, 50] for a more detailed description and analysis. In one dimension, a spline is a piecewise polynomial representation of a smooth curve, connecting a set of points. Each section of the spline between two consecutive

points may be referred to as a 'patch' [50]. Therefore, on each patch, the spline is represented by a polynomial function of arbitrary degree. If this concept is extended to two dimensions, then third-order polynomials are employed in bicubic spline interpolation to generate a bicubic surface defined on a two-dimensional grid of points. Accordingly, in two-dimensional spline interpolation, a patch is defined between four points at its corners. Figure 3 schematically illustrates a patch in a two-dimensional grid.

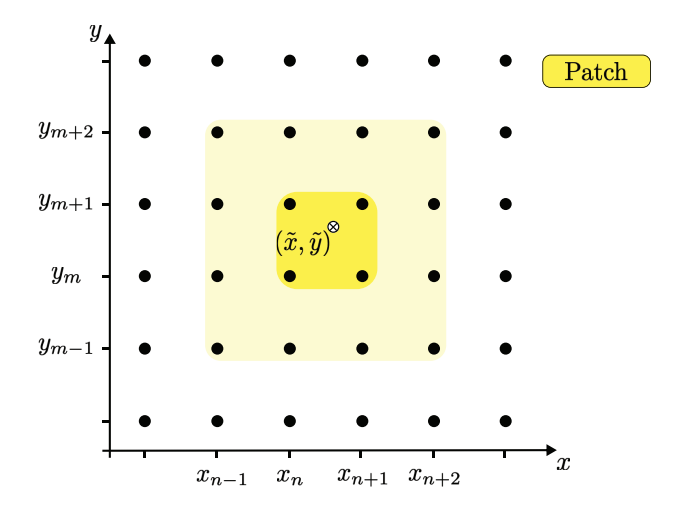


Figure 3: Illustration of sampling points in bicubic spline interpolation: black dots are sample values, the white dot with a cross marks the interpolation point, and the set of points around the patch considered to meet the required conditions. This is a simplified example.

In bicubic spline interpolation, the desired interpolating smooth surface  $\hat{G}(r)$  is defined by the following properties [49]:

(i)  $\hat{G}(\mathbf{r})$  fulfils the interpolation conditions

$$\hat{G}(\mathbf{r}) = \hat{G}(\mathbf{r}_{n,m})$$
, when  $\mathbf{r} = \mathbf{r}_{n,m}$ ,  $\forall n, m$ 

- (ii) Over the whole spatial domain,  $\hat{G}$  is continuously differentiable and  $\partial^2 \hat{G}/\partial x \partial y$  is continuous.
- (iii) In each patch  $\mathcal{P}_{n,m} = \{(x,y) : x_n \le x \le x_{n+1}, y_m \le y \le y_{m+1}\}$  the spline  $\hat{G}$  is defined as a bicubic polynomial, i.e.,

$$\hat{G}(\mathbf{r}) = \sum_{t=0}^{3} \sum_{s=0}^{3} a_{t,s}^{n,m} (x - x_n)^t (y - y_m)^s$$
 (12)

for  $r \in \mathcal{P}_{n,m}$ ,  $\forall n, m$ .

(iv)  $\hat{G}$  fulfils certain boundary conditions.

Equation (12) shows that the interpolation problem is addressed patch by patch by imposing position continuity conditions [50]. The 16 coefficients  $a_{t,s}^{n,m}$  in Equation (12) must be determined so that  $\hat{G}$  meets the properties (*i*) and (*ii*) on each patch  $\mathcal{P}_{n,m}$ . The former property is attained by posing  $a_{0,0}^{n,m} = \hat{G}(\mathbf{r}_{n,m})$  (four conditions), while the latter property is fulfilled by imposing the continuity of the first-order partial derivatives (eight conditions) and mixed second-order partial derivatives (four conditions) at the inner grid points. These derivatives are typically estimated with finite-difference approximations, one-dimensional cubic splines or other interpolation methods involving the four patch points and other surrounding points [49]. Figure 3 shows which grid nodes are involved in bicubic spline when first-order finite-difference approximations are employed to approximate the first-order partial and mixed second-order

partial derivatives. Such approximations introduce relationships between the coefficients  $a_{t,s}^{n,m}$  over each patch, and consequently across the entire spatial domain. Therefore, the values taken by  $\hat{G}(\mathbf{r}_{n,m})$  at each grid node, together with its estimated first-order partial derivatives and mixed second-order partial derivatives, can be employed to determine the coefficients  $a_{t,s}^{n,m}$  using an inverse matrix approach, as long as boundary conditions are provided, thereby ensuring that the matrix to be inverted is square. If N and M represent the number of sample points along the x and y axes, respectively, then 2N + 2M + 4 boundary conditions must be specified [50]. There are several boundary conditions for parametric surfaces, the best known being the free end conditions and the 'not-a-knot' end conditions [50]. It is important to notice that, in a practical scenario, the  $a_{t,s}^{n,m}$  coefficients for each patch can be pre-determined and saved in a look up table. Therefore, once computed, they can be readily used to evaluate  $\hat{G}$  at position  $\tilde{r}$ . In conclusion, condition (ii) illustrates a fundamental property of spline interpolation. In contrast to two-dimensional HD interpolation, bicubic spline ensures continuity of the first derivatives across the entire interpolating surface, with the exception of the domain boundaries. This feature serves to enhance the accuracy of interpolation and provides an explanation as to why polynomial interpolation has lost much of its importance after the introduction of interpolating splines [43].

## 4. The effect of interpolation on the plant modelling error

The interpolation methods presented in the previous section have been employed to estimate the plant responses for different head positions, and to examine the global statistical trend of the interpolation error. The results of this investigation are presented in two distinct parts: The first part analyses the interpolation error associated with the interpolation of head translations, while the second part discusses the effect of interpolation between head rotations. Specifically, interpolation between head translations has been performed at all 108 midpoints of the grid with uniform 5 cm spacing, and at all the 138 inner points of the grid with uniform 10 cm spacing. The interpolation between head rotations has been carried out at angles of  $\pm 9^{\circ}$ ,  $\pm 18^{\circ}$ , with the resulting interpolation error evaluated at each position on the 5 cm grid. As for interpolation between head translations, this approach assumes knowledge of the plant responses,  $\hat{G}$ , only at grid positions spaced 5 cm from each other. The magnitude and phase interpolation errors are calculated for each target position respectively as

$$\epsilon(\widetilde{r},\widetilde{\theta})|_{dB} = \left| 20 \log_{10} \left| \frac{\hat{G}(\widetilde{r},\widetilde{\theta})}{\hat{G}(\widetilde{r},\widetilde{\theta})} \right| \right|$$
 (13a)

$$\epsilon(\widetilde{r},\widetilde{\theta})|_{\angle} = \left| \angle \left[ \hat{G}(\widetilde{r},\widetilde{\theta}) \cdot \hat{G}^*(\widetilde{r},\widetilde{\theta}) \right] \right|. \tag{13b}$$

These values are then averaged over the set of all target grid positions, and the variation over the grid is analysed.

## 4.1. Plant modelling errors for interpolation between head translations

The various interpolation strategies described in Section 3 are applied to head translations assuming that the head is in its natural angular orientation, i.e.  $\tilde{\theta}=0^{\circ}$ . NN interpolation is carried out by considering the 'most accurate' nearest neighbour, which is calculated for each response as discussed in Section 3.1. IDW is implemented by setting  $\gamma=4$ , as recommended in [43, 44]. Two-dimensional HD interpolation of degree 2 and 3 is realised by performing constant extrapolation at the grid boundaries. Lastly, Bicubic Spline interpolation is realised by implementing nota-knot boundary conditions [50]. Figure 4 presents the magnitude and phase interpolation errors associated with the responses between the left secondary loudspeaker and the two ears when interpolation is performed using plant responses at grid nodes spaced 5 cm apart. The solid line illustrates the mean of the interpolation error evaluated over the set of 108 target grid positions, while the bounds of the shaded region are defined by the 10th and 90th percentiles. Figure 4 illustrates that the mean magnitude and phase interpolation errors are respectively below 4 dB and 30° for NN interpolation, and below 2 dB and 10° for the remaining interpolation strategies. Furthermore, Figure 4 reveals that the trends in the interpolation errors associated with the ipsilateral and contralateral paths are similar below 1 kHz for all of the interpolation strategies excluding NN, with a monotonic increase in the error over frequency. For the NN case, the ipsilateral magnitude interpolation error deviates from this pattern and is relatively constant with frequency. Above 1 kHz, the interpolation error for the contralateral paths exhibits an irregular trend. This result, which has also

been observed in other studies where HRTF interpolation has been conducted [26], is primarily attributed to diffraction effects caused by the head [51]. In conclusion, from the results presented in Figure 4 it emerges that the bicubic spline and bicubic HD interpolation strategies achieve similarly low levels of error. This is followed by biquadratic and bilinear HD interpolation strategies and the IDW approach, although, as noted, the magnitude and phase errors for all strategies except NN are relatively small.

The results presented in Figure 4 do not show whether the selected grid spacing of 5 cm represents a reasonable compromise between achieving accurate plant models and minimising the number of stored plant responses used in the interpolation. To investigate this further, the analysis was repeated using the 10 cm grid spacing. In this case, the set of 138 ground truths also included grid nodes located at multiples of 5 cm from the nominal position. Figure 5 shows the average and statistical dispersion of magnitude and phase interpolation errors when biquadratic HD interpolation  $(\delta = 2)$  is applied to plant responses associated with grid spacings of 10 cm and 5 cm. The selected interpolation method is the most appropriate choice for the 10 cm grid, since more accurate methods (HD with  $\delta = 3$  and bicubic spline) are significantly affected by the limited number of available points in the surge direction in this case. The results show that, at the ipsilateral ear, the deviation between interpolation errors increases monotonically with frequency, reaching 1.0 dB at 1000 Hz and 3.5 dB at 1500 Hz for the magnitude response, and 5° at 1000 Hz and approximately 15° at 1500 Hz for the phase response. At the contralateral ear, the deviation varies less regularly, though the overall trend still shows an increase with frequency. Similar patterns are observed for the other interpolation methods, but these have been omitted here for brevity. As outlined in [3] regarding the stability of the active headrest, this analysis demonstrates that increasing grid resolution generally increases the upper frequency limit at which the interpolation error reaches a given value. Having demonstrated how the accuracy degrades with a decreasing grid resolution, as previously explored without interpolation in [3], in the following sections the results will focus on the case with a 5 cm grid spacing.

## 4.2. Plant modelling errors for interpolation between head rotations

To compare the different interpolation strategies applied to head rotations, they have each been applied to head rotations at each position on the 5 cm grid. As interpolation is tested at target head angles of ±9°, ±18°, by interpolating responses measured at  $0^{\circ}$  and  $\pm 27^{\circ}$ , NN interpolation has been implemented without the necessity of selecting the 'most accurate' nearest neighbour. Furthermore, quadratic and cubic HD interpolation have not be considered in this analysis, because their implementation would require extrapolation methods to estimate plant responses at  $\pm 54^{\circ}$ and 81°. The extrapolation error would be high in this case, affecting the interpolation error and the objective of the analysis. IDW is implemented by setting  $\gamma = 2$ , which increases the contribution of the closest plant responses. This decision was made based on the findings presented in [3], which indicate that head rotations alone introduce lower levels of plant response variation compared to translational head movement. Lastly, cubic spline interpolation is again realised using not-a-knot boundary conditions. Figure 6 presents the magnitude and phase interpolation errors related to the responses between the left secondary loudspeaker and the two ears. The solid lines represent the mean of the interpolation error evaluated over the set of 180 head configurations (45 target grid positions and four different head rotations), while the shaded regions are defined by the 10th and 90th percentiles. The overall interpolation error trends are comparable to those observed for interpolation of head translations in Figure 4. The main notable difference occurs in the magnitude error for the ipsilateral, direct path where there is a lower increase in the error with frequency, although the NN strategy shows a similar frequency independent behaviour in this case. Nevertheless, the interpolation strategies that give the most accurate plant responses are cubic spline and linear interpolation. However, the error level for cubic spline is higher than that observed for two-dimensional cubic spline in the case of head translations, which is due to the necessity of implementing boundary conditions in the rotational case, which require the estimation of  $\hat{G}$ at wide angles (±54°), affecting the final estimate. The trend in the interpolation error for the contralateral responses suggests that, above 1.5 kHz, plant responses measured at ±9° and ±18° should themselves be interpolated to estimate the plant responses at intermediate angles.

# 5. The effect of interpolation on control performance

The results presented in the previous section have shown valuable insight into the plant estimation error associated with each interpolation strategy for translational and rotational head movements. In general, the relative levels of

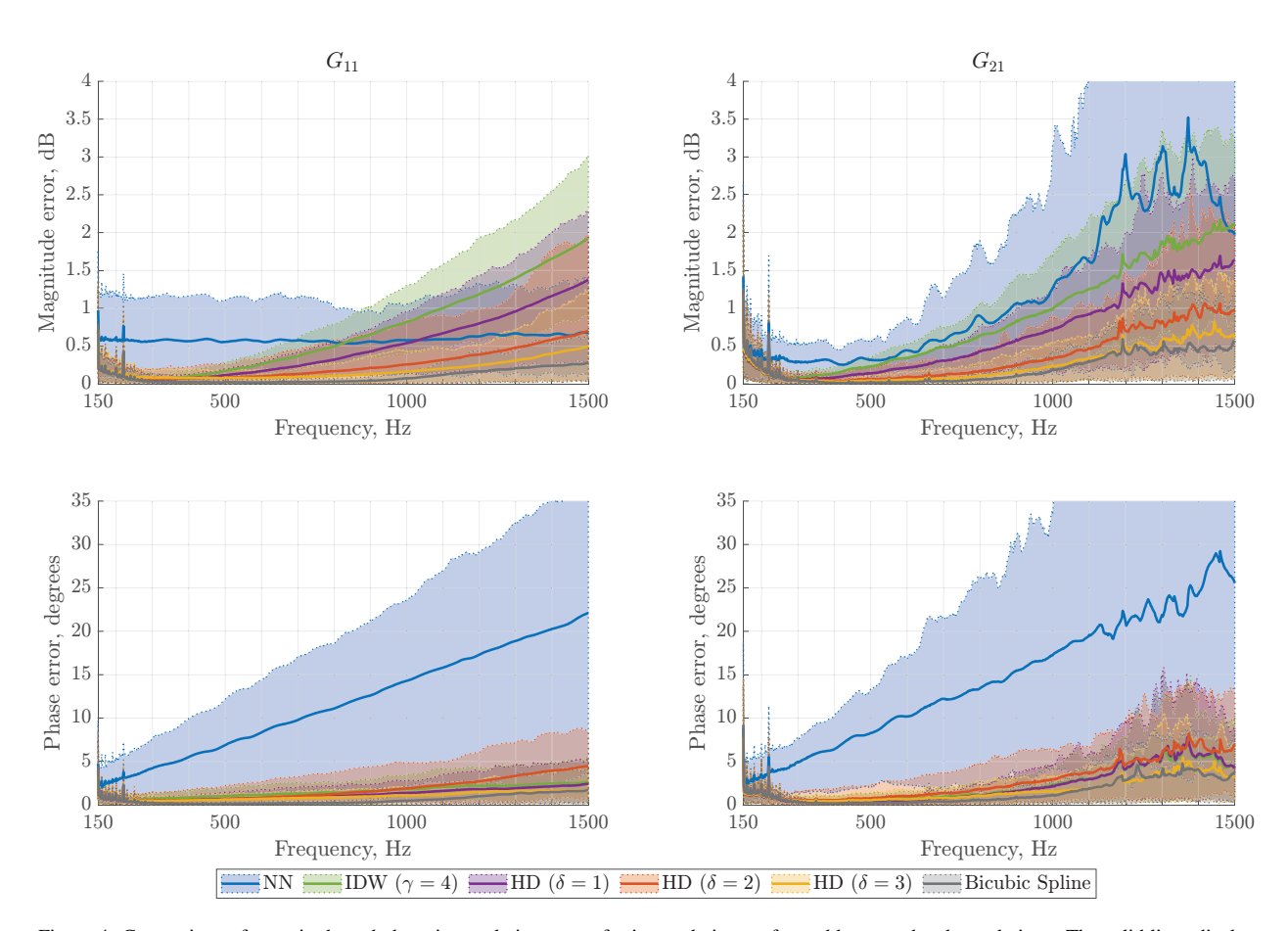


Figure 4: Comparison of magnitude and phase interpolation errors for interpolation performed between head translations. The solid lines display the mean of the interpolation error, while the shaded region is bounded between the 10th and 90th percentiles. The interpolation strategies tested are Nearest Neighbour (NN) interpolation, Inverse Distance Weighting (IDW) interpolation (with power parameter,  $\gamma = 4$ ), High-Degree (HD) interpolation with  $\delta = 1, 2$ , and 3, and Bicubic Spline interpolation.

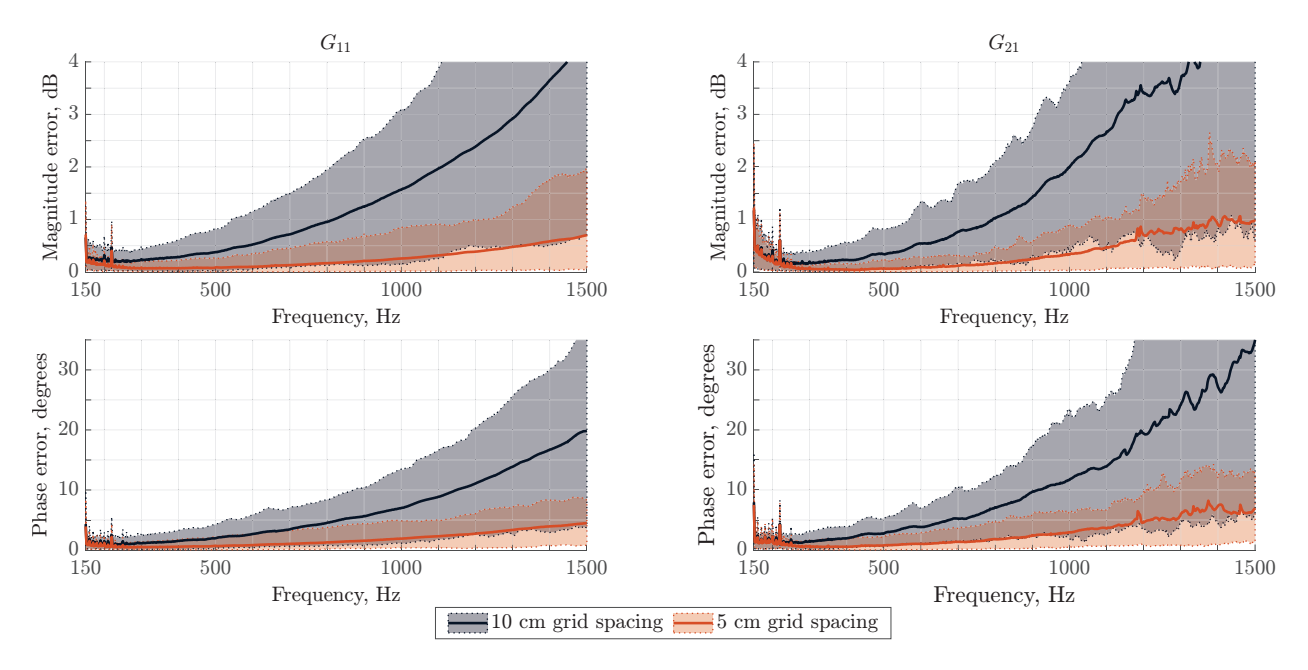


Figure 5: Comparison of magnitude and phase interpolation errors for interpolation performed between head translations with biquadratic HD interpolation ( $\delta = 2$ ). The solid lines display the mean of the interpolation error, while the shaded region is bounded between the 10th and 90th percentiles. The interpolation method is tested for two different grid spacings, i.e., 10 cm and 5 cm.

error for all cases, perhaps excluding NN, are relatively small and decrease with increasing grid spacing, however, it is pertinent to investigate how the plant response interpolation errors affect the behaviour of the controller. Investigation into the behaviour of the controller is separated into two parts: firstly, the effect of the plant model interpolation strategies on the conditioning of the controller is considered, which can be related to the robustness of the controller to practical uncertainties; and secondly, the control attenuation achieved by the controller is evaluated for the different head movements considered when the different interpolation strategies are applied. In both cases, the analysis results are presented exclusively for interpolation using the 5 cm grid spacing.

## 5.1. The effect of plant model interpolation on controller conditioning

In assessing the practical performance of control systems it is important to understand how they will perform in the presence of system variation or uncertainty. This is a complex area of research, but a reliable indication of control system robustness for the optimal tonal feedforward controller assumed here can be conveniently provided by analysing the conditioning of the estimated plant models with respect to matrix inversion [13]. The conditioning of the interpolated plant responses for each interpolation strategy has been studied by calculating the condition number at each grid target position as [52, 53]

$$\kappa(\omega) = \frac{\lambda_{\text{max}}(\omega)}{\lambda_{\text{min}}(\omega)},\tag{14}$$

where  $\lambda$  are the eigenvalues of the matrix  $\hat{\boldsymbol{G}}^H \hat{\boldsymbol{G}}$ , which is inverted in the calculation of the optimal control signals according to Equation (4). The condition number,  $\kappa(\omega)$ , is an important metric to consider, since it is directly linked to the sensitivity of the optimal control signal vector,  $\hat{\boldsymbol{u}}$ , to error in either the measurement of the complex disturbance vector or the plant response [52]. In other words, at frequencies where  $\hat{\boldsymbol{G}}$  is ill-conditioned, the relative error in  $\hat{\boldsymbol{u}}$  will be very high even for small errors in the assumed disturbance or plant responses and the control performance will be severely impacted [53]. Therefore, presenting the condition number for each interpolation strategy, in terms of the average value over all target grid positions, will provide insight into the relative robustness achieved by the different interpolation strategies.

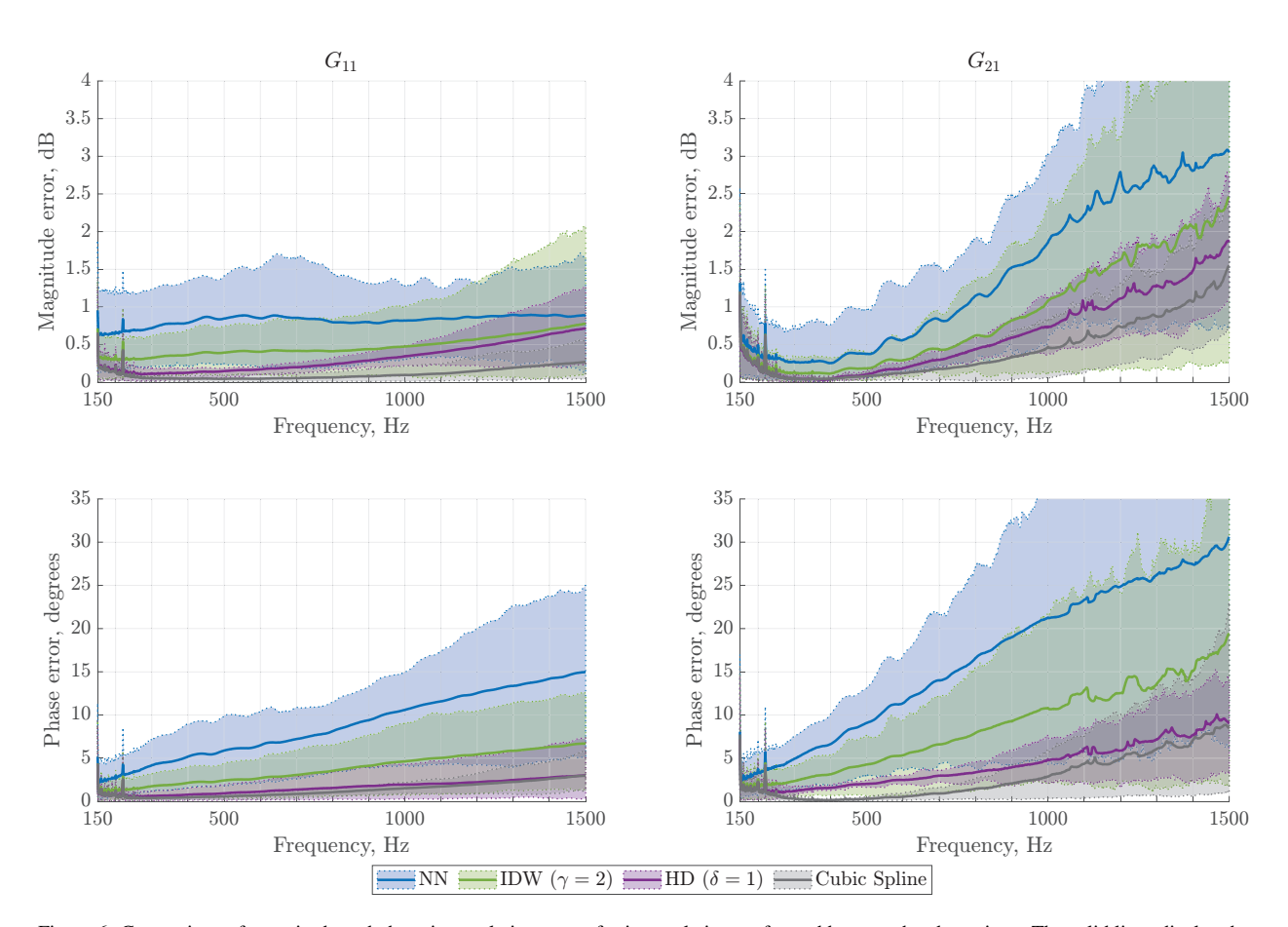
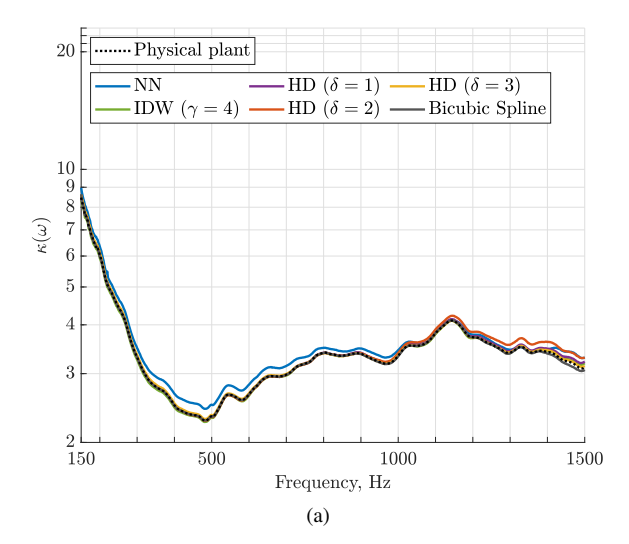


Figure 6: Comparison of magnitude and phase interpolation errors for interpolation performed between head rotations. The solid lines display the mean of the interpolation error, while the shaded region is bounded between the 10th and 90th percentiles. The interpolation strategies tested are Nearest Neighbour (NN) interpolation, Inverse Distance Weighting (IDW) interpolation (with power parameter,  $\gamma = 2$ ), linear High-Degree (HD) interpolation ( $\delta = 1$ ), and Cubic Spline interpolation.



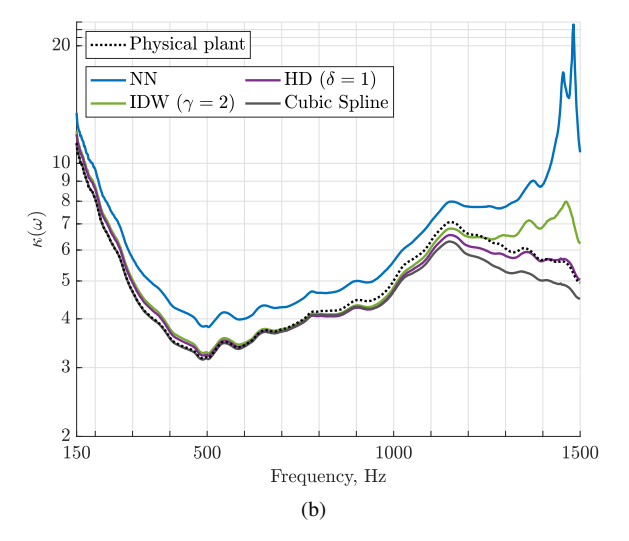


Figure 7: The averaged condition number, calculated according to Equation (14) for the plant models estimated using the considered interpolation methods for head translations (a) and head rotations (b). The results are presented for Nearest Neighbour (NN) interpolation, Inverse Distance Weighting (IDW) interpolation, High-Degree (HD) interpolation, and Cubic Spline interpolation.

In the first instance, the condition number calculated according to Equation (14) and averaged across either the head translations or rotations for the different interpolation strategies is illustrated in Figure 7. Figure 7a presents the condition number for the case of head translations and, in this case, it can be seen that all presented interpolation strategies show similar behaviour. This result indicates that the interpolation strategies that offer lower plant modelling errors, as shown in Section 4, such as bicubic spline and two-dimensional HD interpolation, achieve high quality interpolation without introducing poor conditioning. The selected strategies can therefore be expected to improve the plant modelling accuracy without reducing the robustness of the controller. Figure 7b presents the condition number for the various interpolation strategies applied to head rotation. These results interestingly show that the more accurate interpolation strategies have a lower condition number and so in this case it appears that interpolation benefits both the performance and, probably, the robustness of the headrest system. This result highlights the potential advantage of utilising interpolation strategies that are more accurate than nearest neighbour interpolation. It is also interesting to compare the results presented in Figures 7a and 7b, which clearly shows that the system is in general more ill-conditioned for head rotations than for translations. Theoretically, the plant matrix is expected to be illconditioned at the poles of the elements of the inverse of  $\hat{G}$ , i.e., at frequencies where its determinant approaches zero. In practice, this occurs at specific grid positions and frequencies where the ipsilateral and contralateral paths have similar magnitudes and their phases coincide, leading to a loss of independence between the two responses. At these frequencies the condition number rises sharply. This effect becomes more pronounced with certain head rotations, as shadowing effects diminish – especially close to the sources – further reducing the difference between similar responses and increasing the condition number. Furthermore, this phenomenon explains the sharp peak around 1450 Hz in the condition number shown in Figure 7b for the NN case, while the condition numbers for the physical and interpolated responses remain unaffected. The NN condition number is calculated using measured plant responses at angles ±27° where the described effect is strong enough to significantly affect the overall average. At smaller angles the effect diminishes and becomes less relevant.

## 5.2. The effect of plant model interpolation on the level of attenuation

To assess how the plant model interpolation strategies described in Section 3 influence the achievable control performance, the attenuation in the disturbance at the physical position of the ears when the plant model,  $\hat{G}$ , is estimated by interpolating the measured plant responses at frequencies between 150 Hz and 1500 Hz has been calculated. The

control attenuation is defined as

$$Attn(\omega, \psi, \beta) = -10 \log_{10} \left( \frac{e^H e}{d^H d} \right)$$
 (15)

where e is given by Equation (1),  $\omega$  is the frequency of the disturbance,  $\psi$  is the position and orientation of the head in space, and  $\beta$  is the effort-weighting parameter. While  $\omega$  and  $\psi$  are inherent variables,  $\beta$  can be selected to reach a trade-off between robustness and control performance, as described in Section 2.2. In this paper, instead of choosing a frequency-independent value of  $\beta$  – which is a relatively straightforward and commonly adopted practice [7, 4] – a frequency-dependent control-effort weighting parameter is determined for each interpolation strategy in order to achieve effective control over frequency and to ensure a fair comparison between the different interpolation strategies. The frequency-dependent value of  $\beta$  has been set for each interpolation strategy as

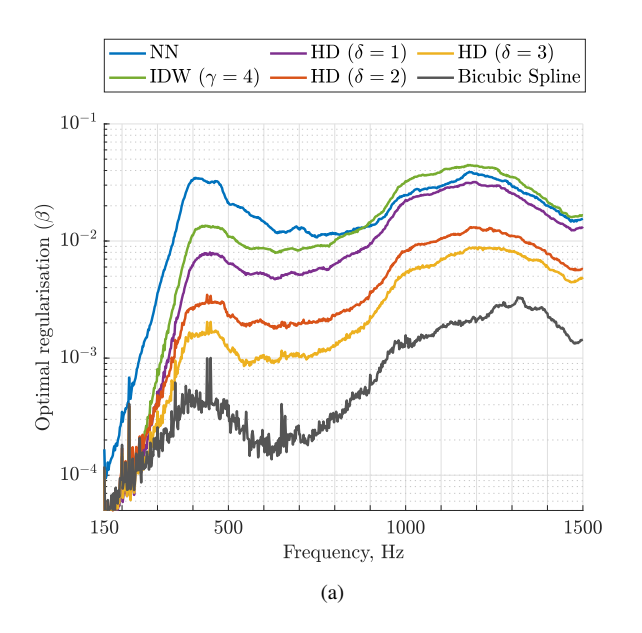
$$\beta(\omega) = \frac{1}{N_{\psi}} \sum_{i} \beta_{i,\max}(\omega) \equiv \frac{1}{N_{\psi}} \sum_{i} \arg\max_{\beta} \{ Attn(\omega, \psi_{i}, \beta) \}$$
 (16)

where  $N_{\psi}$  defines the number of different head configurations that are considered, and  $\beta_{i,\text{max}}$  is the control-effort weighting parameter that gives the maximum attenuation at the *i*-th head position/orientation. In the study, the parameter  $\beta(\omega)$  is determined as in Equation (16) by considering values of  $\beta$  between  $10^{-8}$  and  $2.0 \cdot 10^{-1}$ . Although in practice the control-effort weighting would most likely be constant for all head configurations, in order to explore the differences between translations and rotations, a separate effort-weighting parameter has been calculated for each case.

#### 5.2.1. Head translations

Considering head translations in the first instance, the frequency-dependent value of the control-effort weighting for the controller implemented using each interpolation strategy has first been calculated before assessing the attenuation performance of the controller. To determine the frequency-dependent control-effort weighting parameter for each of the interpolation strategies according to Equation (16), it is necessary to calculate the optimal value of the control-effort weighting at each frequency bin and grid position,  $\beta_{i,\text{max}}$ , which gives the maximum level of attenuation according to Equation (15). Figure 8a shows, for each interpolation strategy, the value of  $\beta(\omega)$  calculated according to Equation (16). These results clearly show that the more accurate interpolation methods (Bicubic Spline, HD  $\delta = 3$ , HD  $\delta = 2$ ) require lower levels of regularisation compared to the less accurate methods (NN, IDW, HD  $\delta = 1$ ). This trend is consistent with the fact that in an ideal scenario, where the plant model is exactly equal to the physical plant response, then the optimal regularisation in terms of maximising the attenuation would be equal to zero. When uncertainties in the plant response exist, it is also interesting to observe how the selected value of  $\beta$  varies with frequency for the different interpolation strategies. From Figure 8a it can be seen that the general trend is quite consistent across the different interpolation strategies. In general, the level of regularisation is relatively small at lower frequencies, which occurs despite the higher condition number shown in Figure 7 at low frequencies due to the increased size of the zone of quiet and reduced sensitivity to positional errors. It is, however, notable that the rate of increase in the magnitude of the regularisation from 150 to 500 Hz is greater for the less accurate interpolation strategies, despite presenting comparable conditioning as observed in Figure 7. At frequencies between around 500 Hz and 1 kHz, the selected effort weighting parameter value decreases, reaching a local minimum, and then increases again at frequencies where head shadowing effects occur; this trend is consistent with the condition number shown in Figure 7. However, it is relevant to highlight that despite the relatively consistent condition number across the different interpolation strategies, the level of regularisation for each strategy differs quite significantly, following more closely the differences in the level of the plant modelling errors explored in Section 4.

Having tuned the regularisation used for the controllers utilising the plant models calculated using each interpolation strategy, it is then important to evaluate the attenuation in the primary disturbance achieved across all translational head positions. Figure 8b shows the attenuation calculated according to Equation (15), where the control-effort weighting parameter has been set according to Equation (16). The solid lines in this figure show the average attenuation achieved across all head translations and the shaded regions are bounded by the 10th and 90th percentile values. In addition, the corresponding results are also presented for the case without head-tracking, where the plant model,  $\hat{G}$ , is equal to the plant corresponding to the nominal position, A, as shown in Figure 1a, regardless of the actual head position. From these results it is clear that head-tracking significantly improves the level of achievable



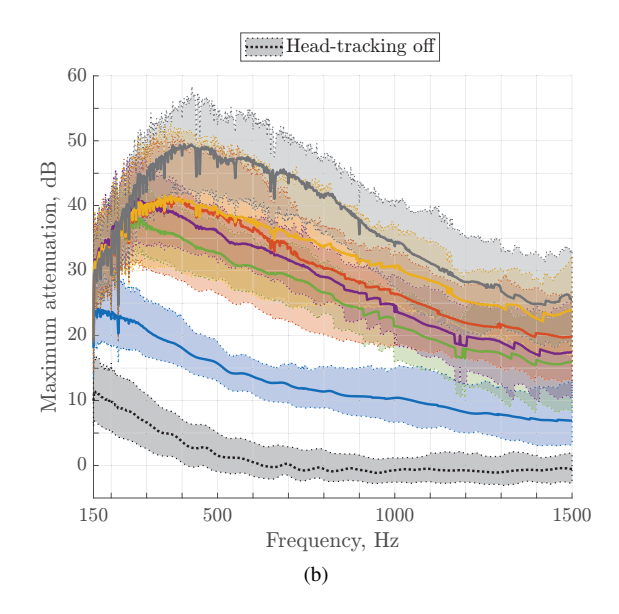
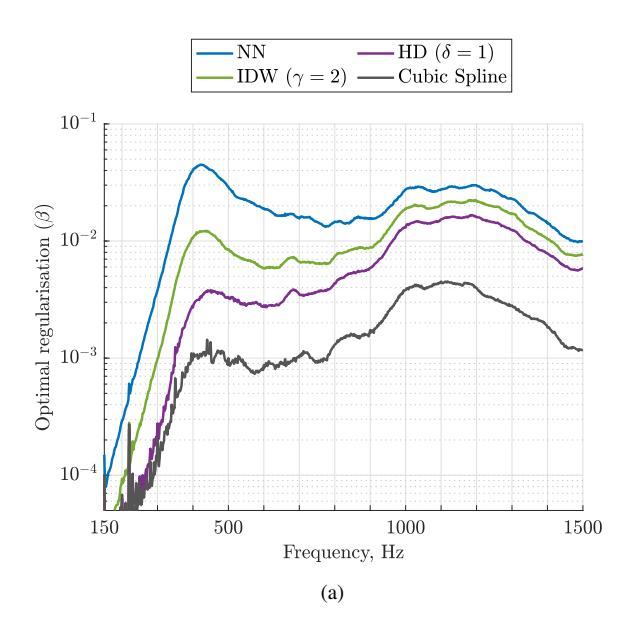


Figure 8: For interpolation between head translations, (a) shows the values of  $\beta$  over frequency calculated according to Equation (16), and (b) shows the control attenuation achieved on average across the range of head translations when utilising the averaged optimal control-effort parameter. The interpolation strategies tested are Nearest Neighbour (NN) interpolation, Inverse Distance Weighting (IDW) interpolation (with power parameter,  $\gamma = 4$ ), High-Degree (HD) interpolation, and Bicubic Spline interpolation. Note, HD interpolation is performed with three different degrees,  $\delta = 1$  (bilinear interpolation),  $\delta = 2$  (biquadratic interpolation), and  $\delta = 3$  (bicubic intepolation).

attenuation, even when nearest neighbour interpolation is utilised, which is consistent with previous work [7]. In the case of NN interpolation, the average attenuation drops below 10 dB for frequencies above around 1 kHz. Using any of the high-order interpolation strategies considered here significantly increases the level of attenuation across the considered bandwidth. For example, for the bicubic spline interpolation case the average attenuation exceeds 25 dB across the entire considered bandwidth, while for two-dimensional HD with  $\delta = 2$  or  $\delta = 3$  the average attenuation is at least 20 dB across the considered bandwidth. The variation in the performance across head-tracking position is relatively insensitive to the interpolation strategy and this is instead perhaps limited due to the fact that a single frequency-dependent control-effort weighting is used for all head positions. In particular, further analysis showed that the value of  $\beta$  obtained using Equation (16) maximises attenuation when the head is positioned at central positions of the grid. In contrast, the lowest attenuation values occur at the lateral grid positions ( $x = \pm 20$  cm). This suggests that higher levels of regularisation are required in grid regions where plant variations are more significant, requiring more accurate models. In conclusion, it is clear that by using more accurate plant model interpolation can, somewhat unsurprisingly, improve the level of control performance achieved, but what is perhaps interesting is that despite the relatively small magnitude of plant modelling errors in both magnitude and phase described in Section 4 there is quite a significant difference in the levels of control attenuation achieved across the different approaches.

## 5.2.2. Head rotations

Following the results presented in the previous section for head translations, this section presents the corresponding study for head rotations. The results presenting the control-effort weighting parameter calculated according to Equation (16) and the corresponding level of attenuation achieved over the various head rotations are presented in Figure 9. Overall, the results show a similar trend to those for the case of translational movement, although as previously in Section 4.2 only a subset of interpolation methods are utilised. As for head translations, Figure 9 shows that more accurate interpolation strategies (Cubic Spline, HD  $\delta = 1$ ) require less regularisation than less accurate ones (IDW, NN). Furthermore, a similar  $\beta$  variation over frequency is noticeable, with regularisation being low at lower frequencies despite higher conditioning (Figure 7b), and increasing more for less accurate methods between 150 and 500 Hz. At higher frequencies,  $\beta$  dips before rising again with the onset of head shadowing effects, in accordance with the conditioning trends. Nevertheless, the absence of the peak observed in Figure 7b for NN suggests that regu-



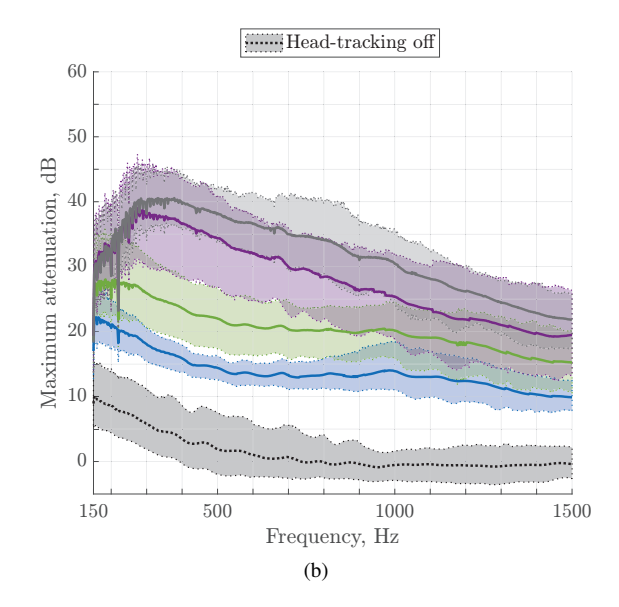


Figure 9: For interpolation between head rotations, (a) shows the values of  $\beta$  over frequency calculated according to Equation (16), and (b) shows the control attenuation achieved on average across the range of head translations when utilising the averaged optimal control-effort parameter. The interpolation strategies tested are Nearest Neighbour (NN) interpolation, Inverse Distance Weighting (IDW) interpolation (with power parameter,  $\gamma = 2$ ), Linear (HD) interpolation ( $\delta = 1$ ), and Cubic Spline interpolation.

larisation levels vary significantly between strategies, reflecting the plant modelling errors more than the conditioning alone. Lastly, Figure 9a shows that the values of  $\beta$  calculated according to Equation (16) are generally different from those shown in Figure 8a. Firstly, it is observed that NN, IDW and linear HD interpolation strategies require the same or less regularisation, probably as a consequence of the better interpolation accuracy obtained between head rotations. Conversely, cubic spline interpolation requires more regularisation due to the extrapolation used to implement the interpolation strategy, which inevitably increases the plant modelling error.

As with the head translations, the obtained values of  $\beta$  are used as in Equation (15) to calculate the average attenuation at each grid position for different head rotations. The corresponding results are presented in Figure 9b, where the solid lines represent the average attenuation across all head rotations, and the shaded areas are bounded by the 10th and 90th percentiles. As noted for the head translations, head-tracking improves attenuation even with NN interpolation; compared to what was observed for Figure 8b, the attenuation level obtained with NN interpolations drops below 10 dB at higher frequencies, in particular above 1.4 kHz. This is a consequence of the fact that head rotations alone result in lower levels of response variation compared to translational head movements. Conversely, Figure 9b illustrates that up to 700 Hz, IDW interpolation results in an attenuation level that is 10 dB lower than that achieved by interpolating between head translations. The limited accuracy of this interpolation method is consistent with the results shown in Figure 6. A similar 10 dB loss in performance is observed with cubic spline interpolation, thereby limiting the attenuation level to below 40 dB. However, as discussed above for Figure 9a, this is due to the extrapolation performed to successfully implement the interpolation strategy, which reduces its accuracy. Linear HD interpolation, on the other hand, results in similar levels of noise reduction. In conclusion, these fluctuations, along with the similarities noted in the retrieved choices of  $\beta$  and the benefit of interpolating between head rotations, which improves control performance despite small plant modelling errors (see Section 4), further suggests that, in a practical scenario, the choice of tuning the headrest system with one single regularisation parameter, which would be common both for plant modelling and interpolation between head translations and rotations, would result in high attenuation levels for accurate interpolation strategies.

#### 6. Conclusions

This paper has presented an investigation into how plant response interpolation can improve the accuracy of plant models used in a  $2 \times 2$  active headrest system subjected to a harmonic disturbance and potentially improve both the robustness and attenuation performance of the control system. In this study it is assumed that the head is free to move and rotate in a plane where plant responses are measured at discrete spatial positions in advance and different interpolation strategies are used to estimate the plant responses in between measured plant response positions. Several interpolation strategies have been introduced and analysed, including nearest neighbour, inverse distance weighting, high-degree and cubic spline interpolation. Their accuracy was assessed in terms of the plant modelling error, indicating that magnitude and phase errors increase at higher frequencies especially due to the difficulty in estimating contralateral paths caused by head shadowing. Nevertheless, on average, the retrieved models deviate from the physical responses by no more than 3.5 dB in magnitude and  $30^{\circ}$  in phase when measured responses are interpolated between grid nodes spaced 5 cm apart. Reducing the grid resolution to 10 cm reduces the number of stored plant responses, but decreases the interpolation accuracy at frequencies above 1000 Hz.

The effect of interpolation on control performance was assessed by analysing the condition number and attenuation at the listener's ears, averaged over all head configurations, when the optimal control signals are calculated. The analysis was performed separately for head translations and rotations. The investigation into the conditioning of the predicted plant models showed that head rotations increase the sensitivity of the control system to plant modelling errors. The headrest system was tuned by adjusting the regularisation separately for translational and rotational head movements. The value of  $\beta$  that maximised attenuation for each frequency and spatial head configuration was then averaged. Results indicated that higher levels of regularisation are required around 500 Hz and at higher frequencies, i.e. at the frequency limit set by the one-tenth wavelength rule and where head shadowing effects occur. It was also observed that accurate interpolation methods require lower levels of regularisation.

The analyses showed that for both head translations and rotations, mean attenuation levels exceed 15 dB across the frequency range when either cubic spline, high degree or inverse distance weighting interpolation are used. Conversely, control performance is poor when nearest neighbour interpolation is used or when the nominal plant matrix is used as the plant model, thus supporting the importance of the conducted analysis. Ultimately, this study has shown that interpolation of plant responses measured at grid points 5 cm apart achieves high noise reduction when accurate interpolation methods are used. Conversely, interpolation between head rotations with a 27° deviation results in less accurate models and lower attenuation levels, particularly when extrapolation is required at boundary nodes. These findings should guide future research where out-of-plane movements and rotations – i.e., heave, pitch, and roll – may be included, together with the validation of the proposed methods in a real-time system and their possible combination with virtual sensing algorithms.

## Acknowledgments

This research was supported in part by the project IN-NOVA: Active reduction of noise transmitted into and from enclosures through encapsulated structures, which has received funding from the European Union's Horizon Europe programme under the Marie Sklodowska-Curie Grant agreement No. 101073037 and from the UK Research and Innovation under the UK government's Horizon Europe funding guarantee (Grant No. EP/X027767/1). J.C. was supported by the Department of Science, Innovation and Technology (DSIT) Royal Academy of Engineering under the Research Chairs and Senior Research Fellowships programme.

## References

- [1] B. Lam, W.-S. Gan, D. Shi, M. Nishimura, S. Elliott, Ten questions concerning active noise control in the built environment, Building and Environment 200 (2021).
- [2] S. Kuo, D. Morgan, Active noise control systems: Algorithms and DSP implementations, Wiley series in telecommunications and signal processing, Wiley, 1996.
- [3] C. K. Lai, J. Cheer, C. Shi, The effect of head-tracking resolution on the stability and performance of a local active noise control headrest system, The Journal of the Acoustical Society of America 157 (2) (2025) 766–777.
- [4] W. Jung, S. J. Elliott, J. Cheer, Combining the remote microphone technique with head-tracking for local active sound control, Journal of the Acoustical Society of America 142 (1) (2017) 298 307.

- [5] B. Rafaely, S. J. Elliott,  $H_2/H_{\infty}$  active control of sound in a headrest: Design and implementation, IEEE Transactions on Control Systems Technology 7 (1) (1999) 79 84.
- [6] M. Pawelczyk, Multiple input-multiple output adaptive feedback control strategies for the active headrest system: Design and real-time implementation, International Journal of Adaptive Control and Signal Processing 17 (10) (2003) 785 800.
- [7] S. J. Elliott, W. Jung, J. Cheer, Head tracking extends local active control of broadband sound to higher frequencies, Scientific Reports 8 (1) (2018).
- [8] J. Buck, S. Jukkert, D. Sachau, Performance evaluation of an active headrest considering non-stationary broadband disturbances and head movement, Journal of the Acoustical Society of America 143 (5) (2018) 2571 2579.
- [9] Z. Zhang, M. Wu, L. Yin, C. Gong, J. Yang, Y. Cao, L. Yang, Robust parallel virtual sensing method for feedback active noise control in a headrest, Mechanical Systems and Signal Processing 178 (2022).
- [10] H. Chen, X. Huang, H. Zou, J. Lu, Research on the robustness of active headrest with virtual microphones to human head rotation, Applied Sciences (Switzerland) 12 (22) (2022).
- [11] J. Y. Oh, H. W. Jung, M. H. Lee, K. H. Lee, Y. J. Kang, Enhancing active noise control of road noise using deep neural network to update secondary path estimate in real time, Mechanical Systems and Signal Processing 206 (2024).
- [12] A. David, S. Elliott, Numerical studies of actively generated quiet zones, Applied Acoustics 41 (1) (1994) 63 79.
- [13] S. J. Elliott, Signal Processing for Active Control, Signal Processing and its Applications, Elsevier Science, 2001.
- [14] D. Moreau, B. Cazzolato, A. Zander, Active noise control at a moving virtual sensor in three-dimensions, Acoustics Australia 36 (3) (2008) 93 96.
- [15] C. Lei, J. Xu, J. Wang, C. Zheng, X. Li, Active headrest with robust performance against head movement, Journal of Low Frequency Noise Vibration and Active Control 34 (3) (2015) 233 250.
- [16] F. Hilgemann, P. Jax, Adaptive feedback active noise control by robust controller interpolation, European Signal Processing Conference, EUSIPCO, 2023, p. 81 85.
- [17] M. I. Michalczyk, Active noise control systems with time varying sound sensor position, Vol. 10, IFAC Secretariat, 2010, p. 44 47.
- [18] C. D. Petersen, A. C. Zander, B. S. Cazzolato, C. H. Hansen, A moving zone of quiet for narrowband noise in a one-dimensional duct using virtual sensing, Journal of the Acoustical Society of America 121 (3) (2007) 1459 1470.
- [19] S. K. Behera, D. P. Das, B. Subudhi, Head movement immune active noise control with head mounted moving microphones, Journal of the Acoustical Society of America 142 (2) (2017) 573 587.
- [20] T. Xiao, X. Qiu, B. Halkon, Ultra-broadband local active noise control with remote acoustic sensing, Scientific Reports 10 (1) (2020).
- [21] Y. Liu, H. Li, H. Zou, Z. Lin, J. Lu, Active headrest combined with a depth camera-based ear-positioning system, The Journal of the Acoustical Society of America 157 (1) (2025) 519–526.
- [22] C. K. Lai, J. Cheer, A comparison between spatial interpolation approaches in a head-tracked active headrest system, in: Forum Acusticum Euronoise 2025, 2025.
- [23] W. Jung, S. J. Elliott, J. Cheer, Local active control of road noise inside a vehicle, Mechanical Systems and Signal Processing 121 (2019) 144
- [24] J. Garcia-Bonito, S. Elliott, Local active control of diffracted diffuse sound fields, Journal of the Acoustical Society of America 98 (2) (1995) 1017 1024.
- [25] J. Garcia-Bonito, S. Elliott, M. Bonilha, Active cancellation of pressure at a point in a pure tone diffracted diffuse sound field, Journal of Sound and Vibration 201 (1) (1997) 43–65.
- [26] J. M. Arend, C. Porschmann, S. Weinzierl, F. Brinkmann, Magnitude-corrected and time-aligned interpolation of head-related transfer functions, IEEE/ACM Transactions on Audio Speech and Language Processing 31 (2023) 3783 3799.
- [27] J. M. Arend, F. Brinkmann, C. Pörschmann, Assessing spherical harmonics interpolation of time-aligned head-related transfer functions, AES: Journal of the Audio Engineering Society 69 (1-2) (2021) 104 117.
- [28] C. Porschmann, J. M. Arend, F. Brinkmann, Directional equalization of sparse head-related transfer function sets for spatial upsampling, IEEE/ACM Transactions on Audio Speech and Language Processing 27 (6) (2019) 1060 1071.
- [29] F. Freeland, L. Biscainho, P. Diniz, Interpositional transfer function for 3d-sound generation, AES: Journal of the Audio Engineering Society 52 (9) (2004) 915 930.
- [30] F. Brinkmann, R. Roden, A. Lindau, S. Weinzierl, Audibility and interpolation of head-above-torso orientation in binaural technology, IEEE Journal on Selected Topics in Signal Processing 9 (5) (2015) 931 942.
- [31] R. Abma, N. Kabir, 3d interpolation of irregular data with a pocs algorithm, GEOPHYSICS 71 (6) (2006) E91-E97.
- [32] Y. Ohtake, A. Belyaev, H.-P. Seidel, 3d scattered data interpolation and approximation with multilevel compactly supported rbfs, Graphical Models 67 (3) (2005) 150–165, special Issue on SMI 2003.
- [33] M. Bozzini, M. Rossini, et al., Testing methods for 3d scattered data interpolation, Multivariate Approximation and Interpolation with Applications 20 (2002).
- [34] S. Koyama, J. Brunnström, H. Ito, N. Ueno, H. Saruwatari, Spatial active noise control based on kernel interpolation of sound field, IEEE/ACM Transactions on Audio, Speech, and Language Processing 29 (2021) 3052–3063. doi:10.1109/TASLP.2021.3107983.
- [35] M. Anthony, M. R. Bai, Active noise control with extended quiet zones using time-domain underdetermined multichannel inverse filters and kernel interpolation, in: Forum Acusticum Euronoise 2025, 2025.
- [36] H. Li, Y. Liu, H. Z. J. Lu, Improving the performance of an active headrest with ear-positioning system using interpolation method, in: Proceedings of the 31st International Congress on Sound and Vibration, 2025.
- [37] A. Roure, A. Albarrazin, S. Douglas, The remote microphone technique for active noise control, in: Proceedings of ACTIVE 99, International symposium, Active control of sound and vibration, Vol. 2, Institute of Noise Control Engineering of the USA, "1999", pp. 1233–1244.
- [38] D. Moreau, B. Cazzolato, A. Zander, C. Petersen, A review of virtual sensing algorithms for active noise control, Algorithms 1 (2) (2008) 69–99.
- [39] S. J. Elliott, J. Cheer, Modeling local active sound control with remote sensors in spatially random pressure fields, The Journal of the Acoustical Society of America 137 (4) (2015) 1936–1946. doi:10.1121/1.4916274.

- [40] O. Kirkeby, P. Nelson, H. Hamada, F. Orduna-Bustamante, Fast deconvolution of multichannel systems using regularization, IEEE Transactions on Speech and Audio Processing 6 (2) (1998) 189–194.
- [41] A. F. Abate, C. Bisogni, A. Castiglione, M. Nappi, Head pose estimation: An extensive survey on recent techniques and applications, Pattern Recognition 127 (2022) 108591.
- [42] D. Shepard, A two-dimensional interpolation function for irregularly-spaced data, Association for Computing Machinery, Inc, 1968, p. 517 524.
- [43] G. Engeln-Müllges, F. Uhlig, Polynomial and Rational Interpolation, Springer Berlin Heidelberg, Berlin, Heidelberg, 1996, pp. 219–249.
- [44] M. Jing, J. Wu, Fast image interpolation using directional inverse distance weighting for real-time applications, Optics Communications 286 (2013) 111–116.
- [45] D. Wang, M. D. Ercegovac, Y. Xiao, Complex function approximation using two-dimensional interpolation, IEEE Transactions on Computers 63 (12) (2014) 2948 2960.
- [46] W. H. Press, S. A. Teukolsky, W. T. Vetterling, B. P. Flannery, Numerical Recipes in C: The Art of Scientific Computing, 2nd Edition, Cambridge University Press, USA, 1992.
- [47] E. Maeland, On the comparison of interpolation methods, IEEE Transactions on Medical Imaging 7 (3) (1988) 213-217.
- [48] R. Sibson, A brief description of natural neighbor interpolation, in: V. Barnett (Ed.), Interpreting Multivariate Data, John Wiley, 1981, pp. 21–36.
- [49] G. Engeln-Müllges, F. Uhlig, Two-Dimensional Splines, Surface Splines, Bézier Splines, B-Splines, Springer Berlin Heidelberg, Berlin, Heidelberg, 1996, pp. 299–339.
- [50] Q. Agrapart, A. Batailly, Cubic and bicubic spline interpolation in python, Tech. rep., École Polytechnique de Montréal (Nov. 2020).
- [51] C. I. Cheng, G. H. Wakefield, Spatial frequency response surfaces: An alternative visualization tool for head-related transfer functions (hrtf's), Vol. 2, IEEE, 1999, p. 961 964.
- [52] P. Nelson, A review of some inverse problems in acoustics, International Journal of Acoustics and Vibration 6 (3) (2001) 118-34.
- [53] G. H. Golub, C. F. V. Loan, Matrix Computations, 4th Edition, Johns Hopkins University Press, 2013.